CrossMark

On the feedback of the winter NAO-driven sea ice anomalies

J. García-Serrano[1,2] · C. Frankignoul[1]

Abstract Satellite-derived sea-ice concentration (SIC) and re-analysed atmospheric data are used to analyse the potential feedback of the North Atlantic Oscillation (NAO)-driven sea-ice anomalies in winter onto the atmosphere during 1979–2013. A maximum covariance analysis shows that this feedback can be detected with monthly data. When SIC leads, the covariability between Atlantic SIC and the Euro-Atlantic atmospheric circulation in February is statistically significant, but shows intra-seasonal differences: the December SIC influence is dominated by anomalies east of Greenland, with maximum amplitude in the Greenland Sea (GS); while the January SIC influence is dominated by anomalies west of Greenland, in the Davis Strait-Labrador Sea (DL) region. The lagged atmospheric anomalies are likewise different. A reduction of SIC over GS in December is followed in February by a negative NAO-like pattern near the surface and a hemispheric signature in the upper-troposphere, thus acting as a negative feedback. On the other hand, a reduction of SIC over DL in January is followed by an atmospheric anomaly over the North Atlantic that projects on the positive phase of the East Atlantic pattern. The dynamics associated with these atmospheric anomalies is described, indicating that transient-eddy activity is likely at work in settling the large-scale patterns. The role of concomitant North Atlantic sea surface temperature anomalies is discussed.

Keywords Sea ice variability · Air–sea interaction · NAO pattern · EA pattern

✉ J. García-Serrano
  javier.garcia@bsc.es

1   LOCEAN/IPSL, Sorbonne Universités (UPMC)-CNRS-IRD-MNHN, Paris, France

2   Earth Sciences Department, Barcelona Supercomputing Center (BSC-CNS), Barcelona, Spain

1 Introduction

The winter North Atlantic Oscillation (NAO) dominates the interannual atmospheric variability in the Euro-Atlantic sector and largely contributes to regional climate variability (e.g. Hurrell et al. 2003; Hurrell and Deser 2009). The winter NAO also drives substantial variability in sea-ice concentration (SIC; e.g. Fang and Wallace 2009; Deser et al. 2000) and sea-surface temperature (SST; e.g. Cayan 1992; Visbeck et al. 2003) via surface wind and heat flux changes. These NAO-induced SIC and SST fluctuations may feedback onto the atmosphere and could thus contribute to climate predictability because of their persistence (e.g. Walsh and Johnson 1979; Frankignoul 1985). The aim of this study is to analyse the observed feedback of the winter NAO-driven sea-ice anomalies and explore its intra-seasonal behaviour.

Previous studies have shown that the winter NAO impact on Atlantic SIC consists of a dipole between the east and west of Greenland, with a positive NAO leading to sea-ice reduction over the Greenland–Barents Seas and sea-ice increase in the Davis Strait-Labrador Sea region, and conversely for a negative NAO (Fang and Wallace 2009; Deser et al. 2000; Wu and Zhang 2010; Frankignoul et al. 2014). Atmospheric general circulation model (AGCM) experiments have been used to investigate the response to this NAO-driven SIC dipole, showing that the equilibrium circulation anomaly projects on the NAO pattern (Alexander et al. 2004; Deser et al. 2004; Magnusdottir et al. 2004) and is reached in about 2 months (Deser et al. 2007). They highlighted the strong SIC-induced surface heat fluxes and the important role of transient-eddies in changing the initial, baroclinic response into the equivalent barotropic NAO-like response. Their results pointed out that this

Table 1 Summary of the statistics for the leading MCA mode between SIC anomalies in December (SIC_{DEC}; top)/January (SIC_{JAN}; bottom) and SLP anomalies over the North Atlantic-European region in February, providing 2- and 1-month lag respectively: squared covariance (SC; $\times 10^8$), squared covariance fraction (SCF; %), and correlation between expansion coefficients (COR); the estimated significance level is given in brackets

	SC	SCF	COR
SIC_{DEC} (lag 2)			
ATL	3.7 (3 %)	64.7 (12 %)	0.60 (13 %)
eG	*3.2 (3 %)*	*73.4 (3 %)*	*0.59 (23 %)*
wG	0.7 (46 %)	52.1 (49 %)	0.39 (51 %)
SIC_{JAN} (lag 1)			
ATL	3.6 (27 %)	49.8 (38 %)	0.49 (50 %)
eG	1.9 (32 %)	52.9 (44 %)	0.54 (40 %)
wG	*2.5 (9 %)*	*69.1 (21 %)*	*0.52 (9 %)*

Different SIC domains are used: the Atlantic basin of the Arctic Ocean (ATL) and its sub-basins, east (eG) and west (wG) of Greenland. The targeted modes of the study, i.e. SIC/eG_{DEC} and SIC/wG_{JAN}, are highlighted in italics

feedback onto the atmosphere is negative: i.e. the NAO polarity of the response is opposite to the one forcing the sea-ice anomalies.

Two studies have established this sea-ice negative feedback from the observations, in agreement with the AGCM results (Strong et al. 2009; Frankignoul et al. 2014). By prescribing the dipolar SIC anomaly and the NAO patterns in an extended winter season (December-to-April), Strong et al. (2009) showed that the feedback operates due to the persistence of the dipole-like SIC anomaly (longer than 2 months). Frankignoul et al. (2014) tackled the problem by making no a priori assumption on the spatial patterns, and obtained a significant NAO-like circulation anomaly lagging the SIC dipole by 6–8 weeks; however, they used the same extended winter season as in Strong et al. (2009), which prevents from isolating the key SIC month for atmospheric predictability. In this study, we refine their analysis and consider separate monthly anomalies in both SIC and the atmosphere, thus focusing on the intra-seasonal time-scale. We find that SIC anomalies east and west of Greenland are associated in different months with distinct circulation anomalies in the Euro-Atlantic sector. We also analyse the dynamics involved in the atmospheric circulation lagging the NAO-driven sea-ice changes.

2 Method and datasets

The potential influence of winter SIC anomalies onto the atmosphere is first identified by a lag maximum covariance analysis (MCA; e.g. Bretherton et al. 1992; Czaja and Frankignoul 2002) between monthly North Atlantic SIC

and sea level pressure (SLP) anomalies. MCA performs a singular value decomposition of the (area-weighted) covariance matrix between two fields, and provides a pair of spatial patterns and associated standardized time-series (hereafter, expansion coefficients) for each covariability mode, which is characterized by its squared covariance (SC), the squared covariance fraction (SCF), and the correlation between expansion coefficients (COR). The statistical significance of the MCA modes is evaluated with a Monte-Carlo test, based on 100 permutations shuffling only the atmospheric field (SLP) with replacement; the significance level is given by the numbers of randomized values that exceed the actual values being tested. As MCA maximizes the covariance, the primary test for statistical significance is the one upon SC (e.g. Gan and Wu 2015); SCF and COR usually yield lower significance levels (see Table 1). Area-averaged SIC indices are also defined to analyse atmospheric anomalies lagging sea-ice changes. For ease of comparison with previous studies, all SIC and MCA-SIC time-series are referred to sea-ice reduction over the target region.

This study uses SIC data from the NOAA/NCDC passive microwave monthly Northern Hemisphere sea-ice concentration record for 1979–2013, provided by the National Snow and Ice Data Center (NSIDC; Comiso 2012). No threshold for absence/presence of sea-ice has been applied, i.e. continuous fractions have been considered. SST data from the NOAA extended reconstructed SST v3b (Smith et al. 2008) is also used. All atmospheric fields are given by the ERA-Interim re-analysis (ERA-int), available at the European Centre for Medium-range Weather Forecasts (ECMWF; Dee et al. 2011). In addition to SLP, monthly geopotential height at 200 hPa (Z200; as representative of the upper-troposphere) and 50 hPa (Z050; as representative of the lower-stratosphere) have been retrieved. Daily fields are used to analyse the role of internal dynamics: the transient-eddy momentum flux ($u'v'$) at 200 hPa is considered to assess the interaction between eddies and mean-flow through barotropic processes (e.g. Hoskins et al. 1983; Trenberth 1986); and, the transient-eddy heat flux ($v'T'$) at 850 hPa is considered to evaluate the impact of baroclinic processes and changes in low-level waves (e.g. Andrews et al. 1987; Wallace et al. 1988). The monthly-mean covariances have been computed from filtered daily data using the 24 h-difference filter (e.g. Wallace et al. 1988; Chang and Fu 2002). To assess the anomalous heating of the lower troposphere through changes in the surface turbulent heat flux, 3-hourly forecast-accumulated sensible and latent heat flux initialized twice a day (00, 12 h) are also employed. All monthly anomalies are calculated by subtracting the corresponding monthly climatology. To reduce the effect of long-term nonlinear trends, a least squares fit at each grid-point is used to remove a third-order polynomial (i.e. cubic

trend) from all data. It was verified that the results were not sensitive to this particular criteria.

3 Results

3.1 Identification of the lagged sea-ice influence

The covariability between Atlantic SIC anomalies in a given month and monthly SLP anomalies is examined for the same extended season as in Strong et al. (2009) and Frankignoul et al. (2014), namely for SIC in December-to-April. Figure 1 summarizes the MCA statistics for SC of the main mode of covariability upon the three different SIC domains considered: the Atlantic basin of the Arctic Ocean (ATL; Fig. 1a) and its sub-basins, east (eG; Fig. 1b) and west (wG; Fig. 1c) of Greenland. The MCA analysis starts at lag zero, i.e. contemporaneous relationship, when the atmospheric forcing of SIC fluctuations is expected to dominate (e.g. Deser et al. 2000; Frankignoul et al. 2014). Consistent with Fig. 5 below, the first MCA mode at lag zero describes the SIC anomalies associated with the NAO forcing (not shown). Positive lags stand for SIC changes leading SLP anomalies. At 2-month lead-time, consistent with the expected response time of the atmosphere to SIC anomalies (e.g. Deser et al. 2007), there is a prominent SC peak between December SIC variability and the Euro-Atlantic atmosphere in February, which is significant at 95 % confidence level and appears to be dominated by SIC anomalies over eG (Fig. 1a, b, green); this lagged relationship is analysed in Sect. 3.2. There is also a potential influence of January SIC variability over wG on the atmospheric circulation of February, which is significant at 90 % confidence level (Fig. 1c, blue); this lagged relationship is discussed in Sect. 3.3. At lead-times longer than the expected atmospheric response time to SIC forcing, there are some indications of a potential influence of SIC variability over wG on the atmosphere in April (Fig. 1c, blue) and July (Fig. 1c, yellow/magenta). As this study focuses on the cold season, these signals are not discussed.

According to Fig. 1, the target months for the rest of the study are December/January for SIC anomalies and January/February for atmospheric anomalies. The first step towards understanding the potential influence of December/January SIC variability on the Euro-Atlantic atmospheric circulation is to assess their persistence. Figure 2 illustrates the local persistence of (detrended) winter SIC anomalies over the Atlantic basin by showing grid-point correlation maps between anomalies in December (left) and January (right), and lagged anomalies. The largest correlations take place in the marginal ice zones, around the climatological sea-ice edge (green contours). At 2-month lag, December SIC anomalies strongly persist in the
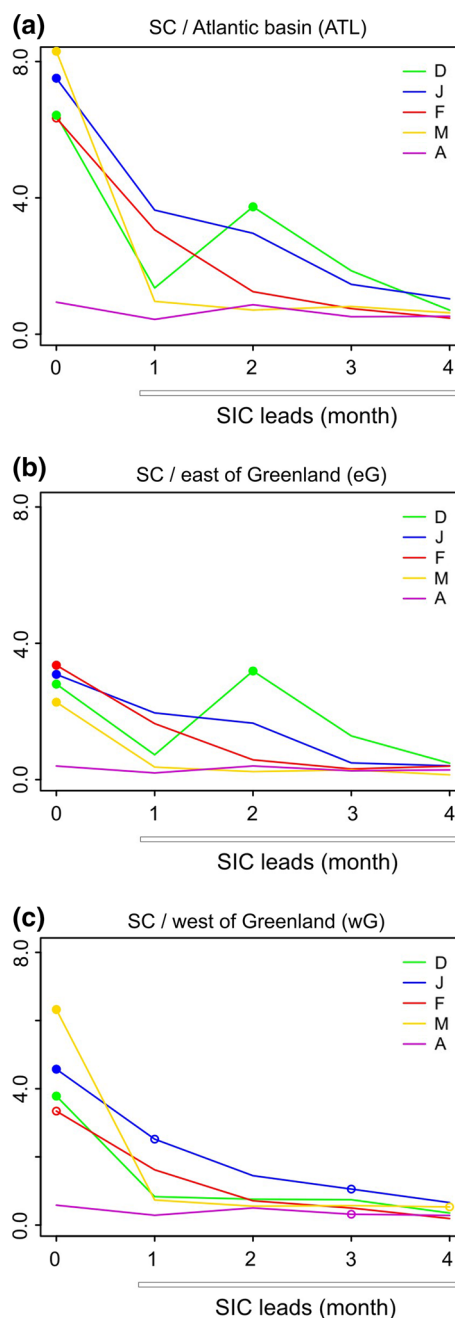

Fig. 1 Squared covariance (SC; $\times 10^8$) of the first MCA mode between monthly detrended SIC anomalies (*coloured lines*) over the Atlantic basin (**a**), east (**b**) and west (**c**) of Greenland, and SLP anomalies over the North Atlantic-European region lagging by 0–4 months; *solid* (*open*) *circle* indicates statistically significant mode at 95 % (90 %) confidence level based on a Monte-Carlo test of 100 permutations shuffling only SLP with replacement

Greenland and Barents Seas and over the Davis Strait, whereas anomalies in the Labrador Sea vanish (Fig. 2a, b). At 1-month lag, January SIC anomalies yield a wider and stronger persistence area west of Greenland than December SIC anomalies (Fig. 2a, c), following the expansion of the

Fig. 2 Grid-point correlation map of detrended SIC anomalies in December (**a**, **b**) and January (**c**) with anomalies 1 (**a**, **c**) or 2 (**b**) months later; *light-green* (*green*) contour stands for the climatological sea-ice edge in the target (*lagged*) month, estimated by the 25 % fraction. Statistically significant areas at 95 % confidence level based on a two-tailed *t* test are contoured. [*bottom*] Climatology of SIC in December (**d**) and January (**e**) over the period 1979–2013; *green contour* stands for the climatological sea-ice edge estimated by the 25 % fraction; *black contour* indicates the isoline of 25 % for SIC standard deviation
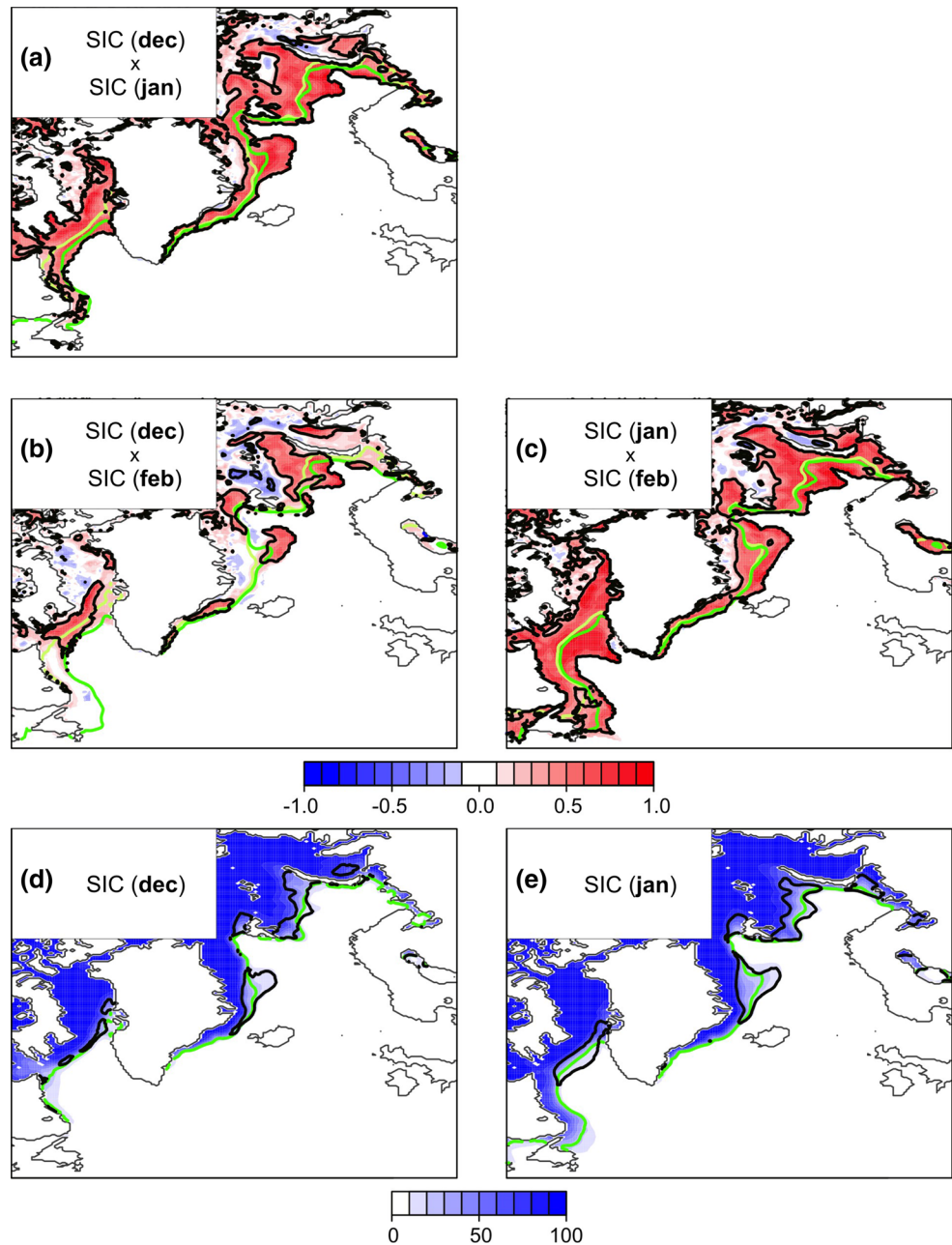
climatological edge and the increase in variability (Fig. 2d, e). These results are in agreement with the long decaying time-scale of the winter NAO-driven SIC anomalies shown by Strong et al. (2009), enabling the detection of its feedback onto the atmosphere later in the season.

3.2 Influence of December sea-ice on the atmosphere

Figure 3 (left) shows the leading MCA mode between SIC anomalies over eG in December and SLP anomalies over the North Atlantic-European region in February (Fig. 1b, green; Table 1). The SIC pattern (Fig. 3a) resembles the well-known dipolar signature induced by a positive NAO

(see Fig. 5c below), with maximum sea-ice reduction in the Greenland Sea (~30 %). The SLP pattern (Fig. 3c) resembles the negative phase of the NAO, which is the first EOF mode of SLP in February (Fig. 4a). This MCA result points out the change in the NAO-like polarity between atmospheric anomalies leading and lagging the December SIC anomalies east of Greenland.

To be independent of the MCA framework, an area-averaged SIC index is considered. The area is 20°W–0°E/68°N–80°N, which is representative of the Greenland Sea (hereafter SIC-GS$_{DEC}$). The associated SIC pattern (Fig. 5a) is nearly identical to the one in Fig. 3a, and the correlation between the respective time-series is 0.92. This pattern
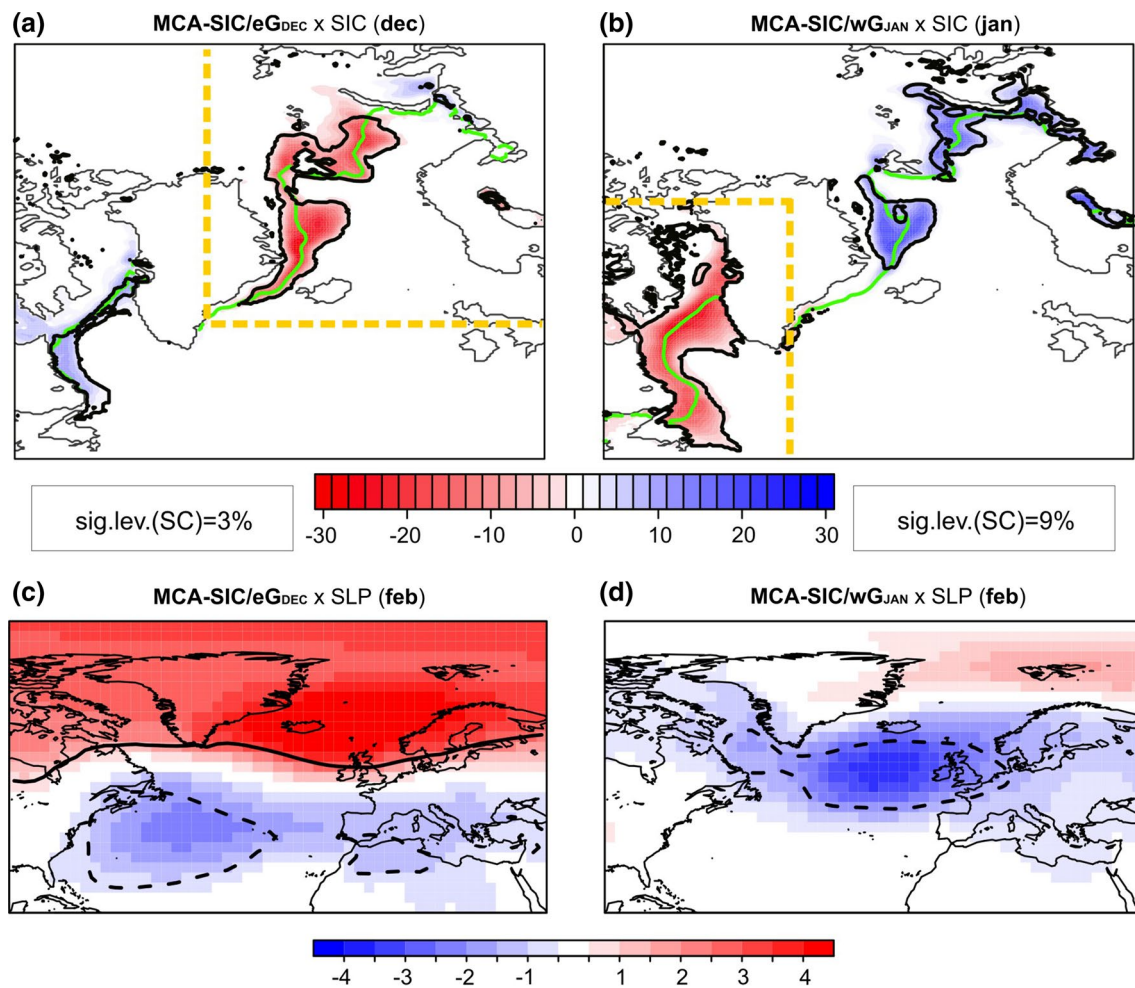
Fig. 3 Leading MCA covariability mode between detrended SIC anomalies (%; *top*) in December east of (eG; **a**)/January west of (wG; **b**) Greenland and SLP anomalies (hPa; *bottom*) in February, providing 2- and 1-month lag respectively; the estimated significance level for the SC of each mode (Fig. 1b, c) is indicated. Shown are regression maps of detrended anomalies onto the corresponding MCA-SIC expansion coefficient; amplitudes correspond to one SD of the time-series. *Green contour* (in *top*) stands for the climatological sea-ice edge estimated by the 25 % fraction; the *yellow box* indicates the SIC region used for the MCA analysis. Statistically significant areas at 95 % confidence level based on a two-tailed *t* test are *contoured*

illustrates the strong coupling of SIC anomalies at both sides of Greenland due to the NAO forcing (Fig. 5c). In the Greenland Sea, the increased heat release to the atmosphere (Fig. 5e) results from the sea-ice reduction, which opens an ice-free ocean region. Elsewhere, the surface heat flux anomalies primarily reflect the imprint of the positive NAO-like pattern (e.g. Cayan 1992).

In January, 1 month later, the SLP anomalies associated with SIC-GS$_{DEC}$ already show hints of a negative NAO-like pattern, with positive anomalies at high latitudes and negative ones at North Atlantic mid-latitudes, although they are weak and not statistically significant (Fig. 6e). The most striking feature is the equivalent-barotropic low over Europe, which has a westward tilt with height suggestive of Rossby wave propagation (Fig. 6-left). The upper-tropospheric anomalies (Fig. 6c) share some similarity with the

transient response to prescribed sea-ice changes reported by Deser et al. (2007). Likewise, the heat flux dipole-like anomaly over eG/wG, with increased/reduced heat release (Fig. 7e), reflects the SIC damping found in other AGCM studies (Alexander et al. 2004; Deser et al. 2004; Magnusdottir et al. 2004). The surface heat flux anomalies over the Gulf Stream region also reflect a negative feedback onto the NAO-related SST anomalies (cf. Figs. 5e with 7e). This suggests that the circulation anomalies in January associated with SIC-GS$_{DEC}$ might be driven or modulated by the sea-ice and associated SST changes (see discussion in Sect. 4).

In February, the negative NAO-like pattern associated with SIC-GS$_{DEC}$ is established (Fig. 6f). This pattern consistently projects on the regional one from the MCA-SIC/eG$_{DEC}$ analysis (Fig. 3c). Interestingly, it is hemispheric
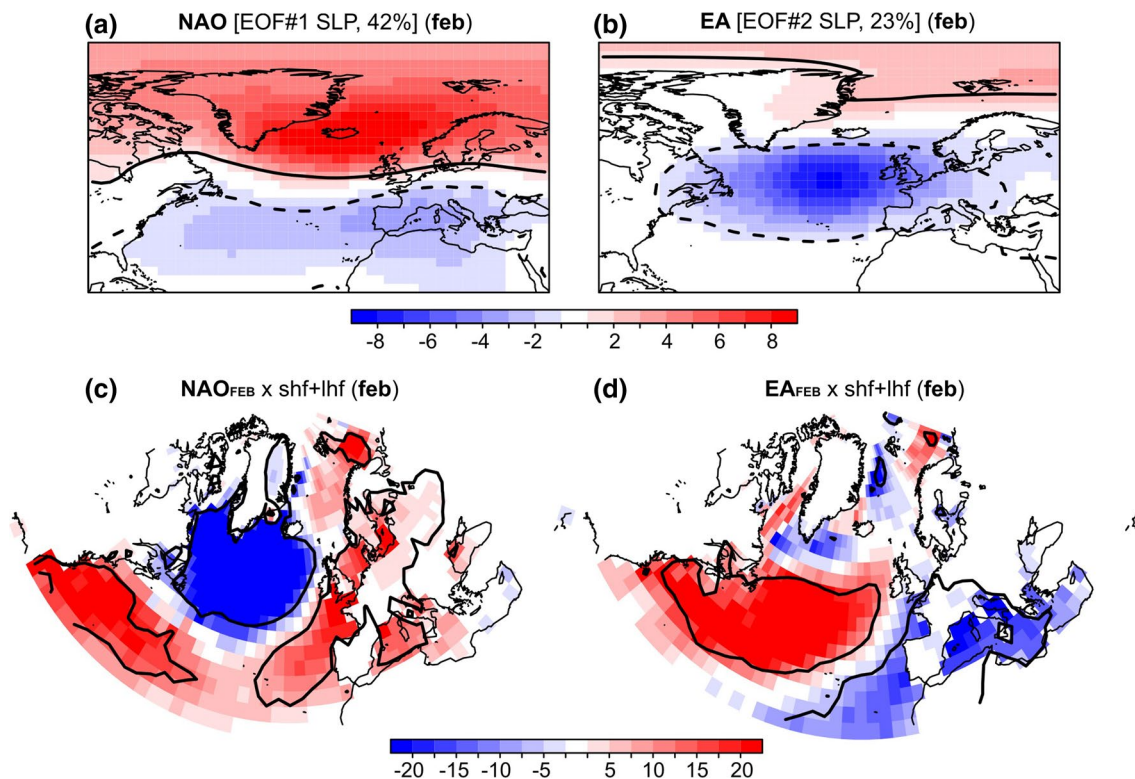
Fig. 4 [*top*] First (**a**) and second (**b**) leading EOF modes of detrended SLP anomalies (hPa) in February over the North Atlantic-European region, corresponding to the NAO (negative phase is shown) and EA patterns respectively; the fraction of explained variance by each mode (%) is indicated in the *title*. [*bottom*] Regression maps of detrended surface turbulent heat flux anomalies (sensible plus latent, W/m^2; upward is positive) onto the NAO (**c**) and EA (**d**) principal components in February. Shown are amplitudes associated with one SD of the corresponding time-series. Statistically significant areas at 95 % confidence level based on a two-tailed *t* test are *contoured*

in scale throughout the troposphere and lower stratosphere (Fig. 6-right), but variations in the polar vortex are barely statistically significant (Fig. 6b). The tropospheric anomalies (Fig. 6d, f) are in agreement with the equilibrium response to prescribed sea-ice forcing in the Atlantic basin from Deser et al. (2007). Composite analysis based on ±1 SD of the SIC-GS$_{DEC}$ index yields similar results (not shown). The imprint of the negative NAO-like pattern dominates the surface heat flux anomalies associated with SIC-GS$_{DEC}$ (cf. Figs. 4c with 7f), although some residual anomalous heat release remains east of Greenland.

Concerning the settling of the NAO-like pattern, from January to February, there is an overall intensification of the eddy activity (Fig. 7, top-middle), suggesting that the positive eddy feedback amplifies and establishes the large-scale atmospheric anomaly (Deser et al. 2004, 2007). Consistent with the negative NAO-like pattern, SIC-GS$_{DEC}$ is associated with a reduction in eddy heat and momentum flux over the western North Atlantic (Fig. 7b, d), indicating a weakening of the jet at its entrance. Over Europe, SIC-GS$_{DEC}$ is associated with an anomalous westerly-momentum deposition to the south (Fig. 7b) and a southward displacement of

low-level waves (Fig. 7d), representing a weakening of the jet at its tail.

3.3 Influence of January sea-ice on the atmosphere

The lagged covariability between January SIC anomalies over wG and the Euro-Atlantic atmospheric circulation in February (Fig. 1c, blue; Table 1) is displayed in Fig. 3-right. The SIC pattern (Fig. 3b) shows a widening of the signal over the Davis Strait-Labrador Sea (DL) region as compared to the thin anomaly in December associated with SIC variability over eG (Figs. 3a, 5a), which reflects the intra-seasonal increase in extent and variance (Fig. 2d, e). The SLP pattern following sea-ice reduction over DL is reminiscent of the East Atlantic (EA) pattern (Fig. 3d), which is the second EOF mode of SLP in February (Fig. 4b). There is thus an intra-seasonal change in the atmospheric circulation lagging SIC anomalies in December (NAO-like; Fig. 3c) and January (EA-like; Fig. 3d).

To assess robustness of the MCA results, an are-averaged SIC index is computed over 65°W–50°W/52°N–68°N, which covers most of the DL region (hereafter
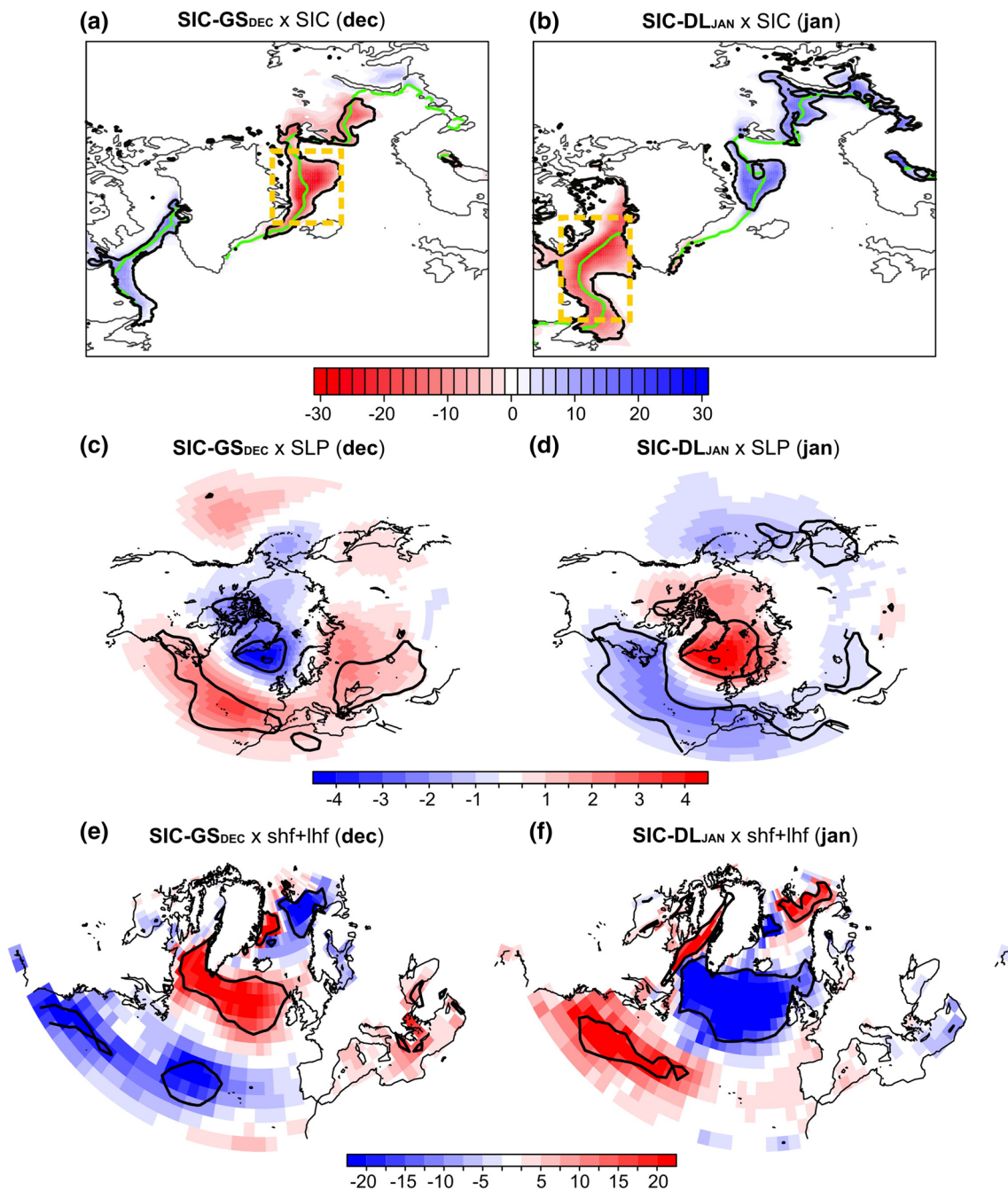
Fig. 5 Regression maps of detrended SIC (%; *top*), SLP (hPa; *middle*), and surface turbulent heat flux (sensible plus latent, W/m^2; upward is positive; *bottom*) anomalies in December onto the SIC-GS$_{DEC}$ index (*left*), and in January onto the SIC-DL$_{JAN}$ index (*right*); amplitudes correspond to one SD of the time-series. *Green contour* (in *top*) stands for the climatological sea-ice edge estimated by the 25 % fraction; the *yellow box* indicates the region used to define the corresponding SIC index. Statistically significant areas at 95 % confidence level based on a two-tailed *t* test are *contoured*

SIC-DL$_{JAN}$). The associated SIC pattern (Fig. 5b) rightly projects on the one in Fig. 3b, since their corresponding time-series are highly correlated (0.99), and it is largely driven by the NAO (Fig. 5d). As before, in addition to the strong NAO imprint in surface heat flux at North Atlantic middle/subpolar latitudes (e.g. Cayan 1992), SIC-DL$_{JAN}$ is associated with an increased heat release over the area where sea-ice has retreated (Fig. 5f).

In February, 1 month later, the anomalous heat release west of Greenland strongly remains (Fig. 8f). SIC-DL$_{JAN}$ recaptures the positive EA-like SLP pattern found with MCA-SIC/wG$_{JAN}$ (Figs. 3d, 8e), which dominates the

Fig. 6 Regression maps of detrended geopotential height anomalies at 50 hPa (Z050, m; *top*) and 200 hPa (Z200, m; *middle*), and SLP anomalies (hPa; *bottom*) in January (*left*) and February (*right*) onto the SIC-GS$_{DEC}$ index; amplitudes correspond to one SD of the time-series. Statistically significant areas at 95 % confidence level based on a two-tailed t test are *contoured*
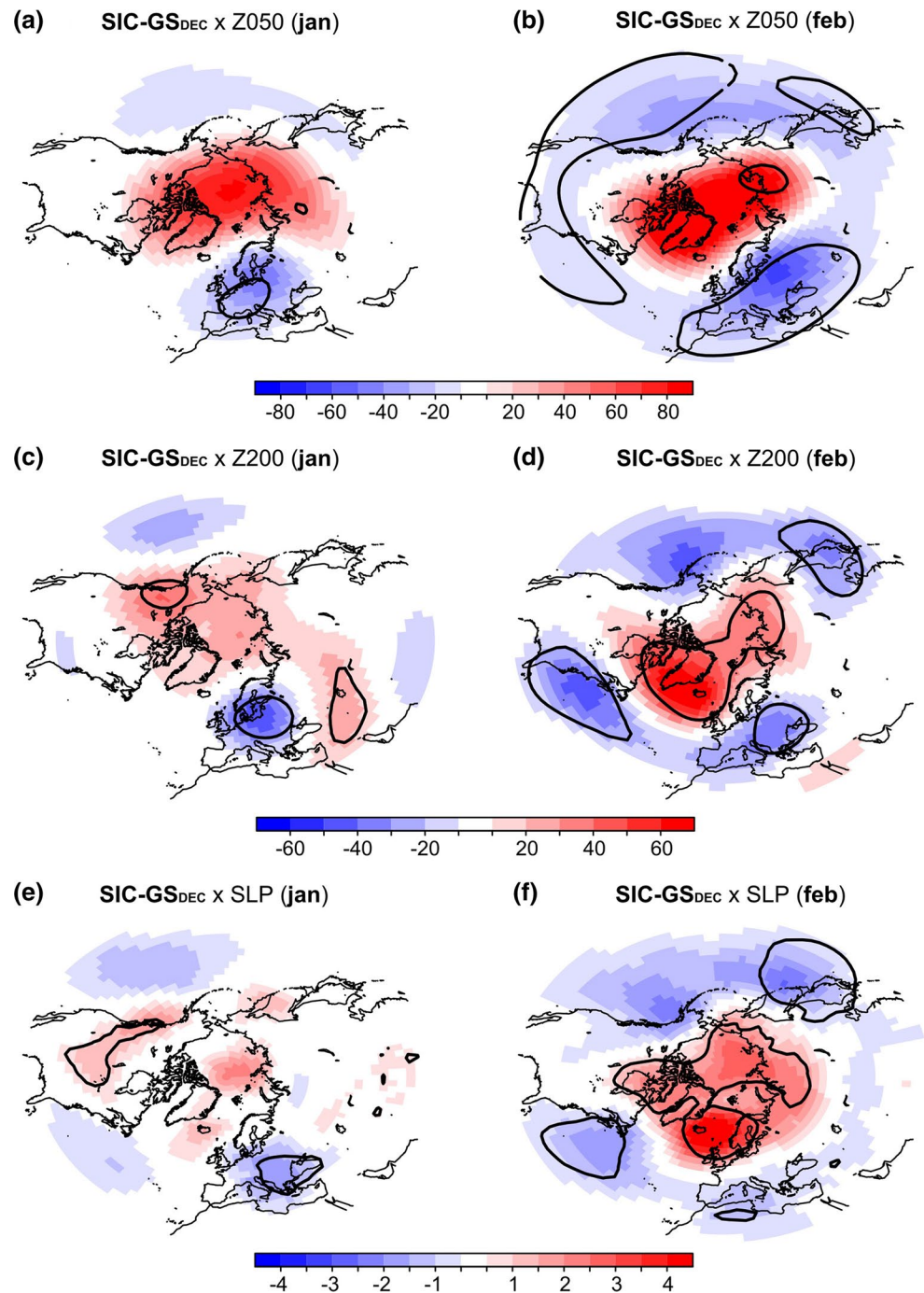
surface heat flux anomalies at North Atlantic mid-latitudes (cf. Figs. 4d with 8f; see also Cayan 1992). The strong heat release over the region of sea-ice reduction more clearly stands out when the latter (obtained by linear regression of the EA principal component) is removed (Fig. 9a). The related atmospheric warming in low levels (below 700 hPa; Fig. 9b) should diminish the meridional temperature gradient and local baroclinicity (e.g. Czaja et al. 2003); a decrease in the eddy heat flux is indeed observed (Fig. 8d). SIC-DL$_{JAN}$ is also associated with decreased

westerly-momentum deposition towards the eddy-driven jet (Fig. 8b). Together, eddy activity is consistent with the settling of the EA-like pattern (e.g. Wettstein and Wallace 2010; Woollings et al. 2010). Note that the 1-month response time suggested by our analysis is in agreement with Ferreira and Frankignoul (2005), who showed that the EA was responding more quickly to boundary forcing than the NAO. At the upper-troposphere (Fig. 8c), the EA-like Z200 pattern associated with SIC-DL$_{JAN}$ shows a dipolar structure confined to the North Atlantic basin, which is broadly
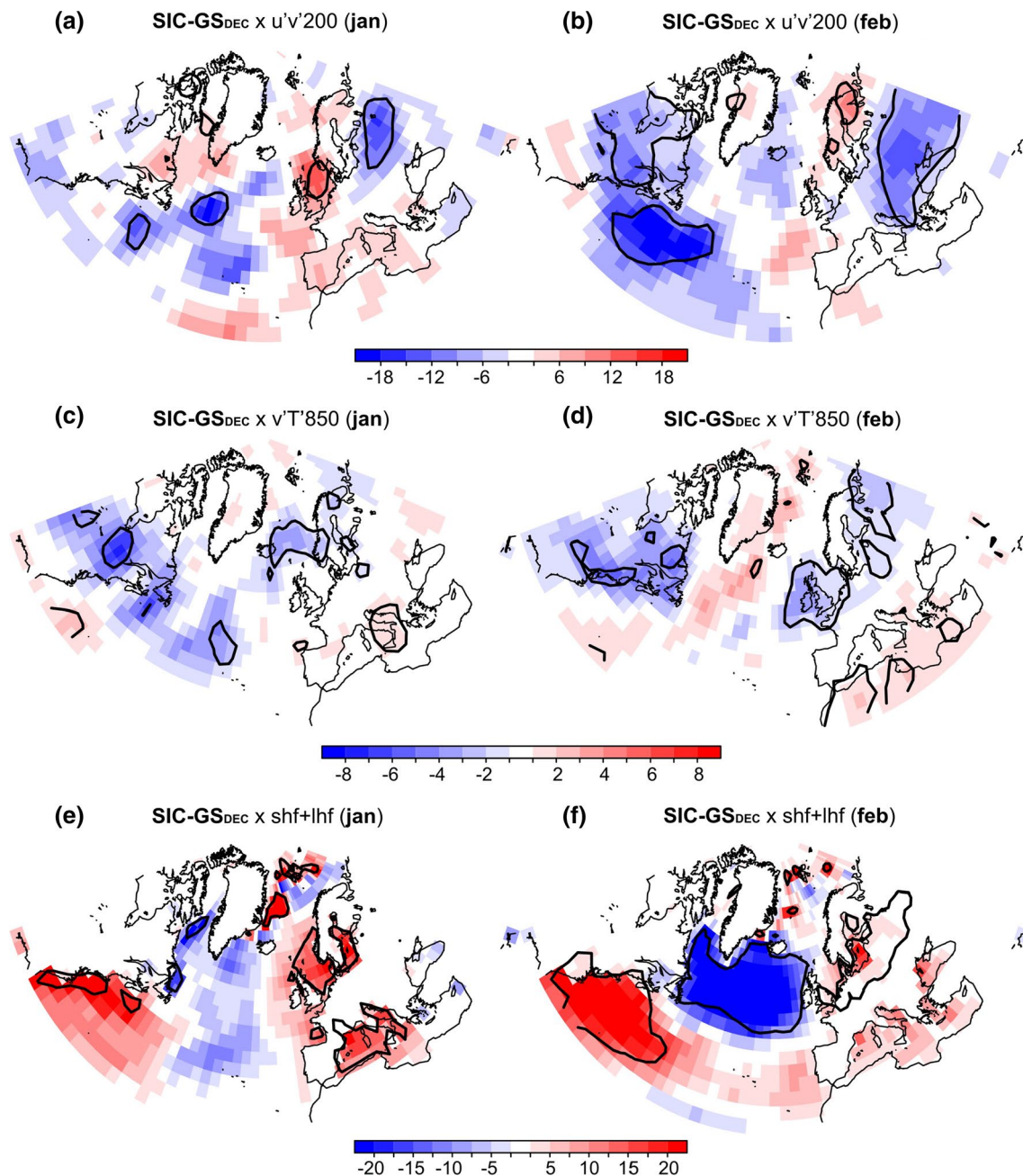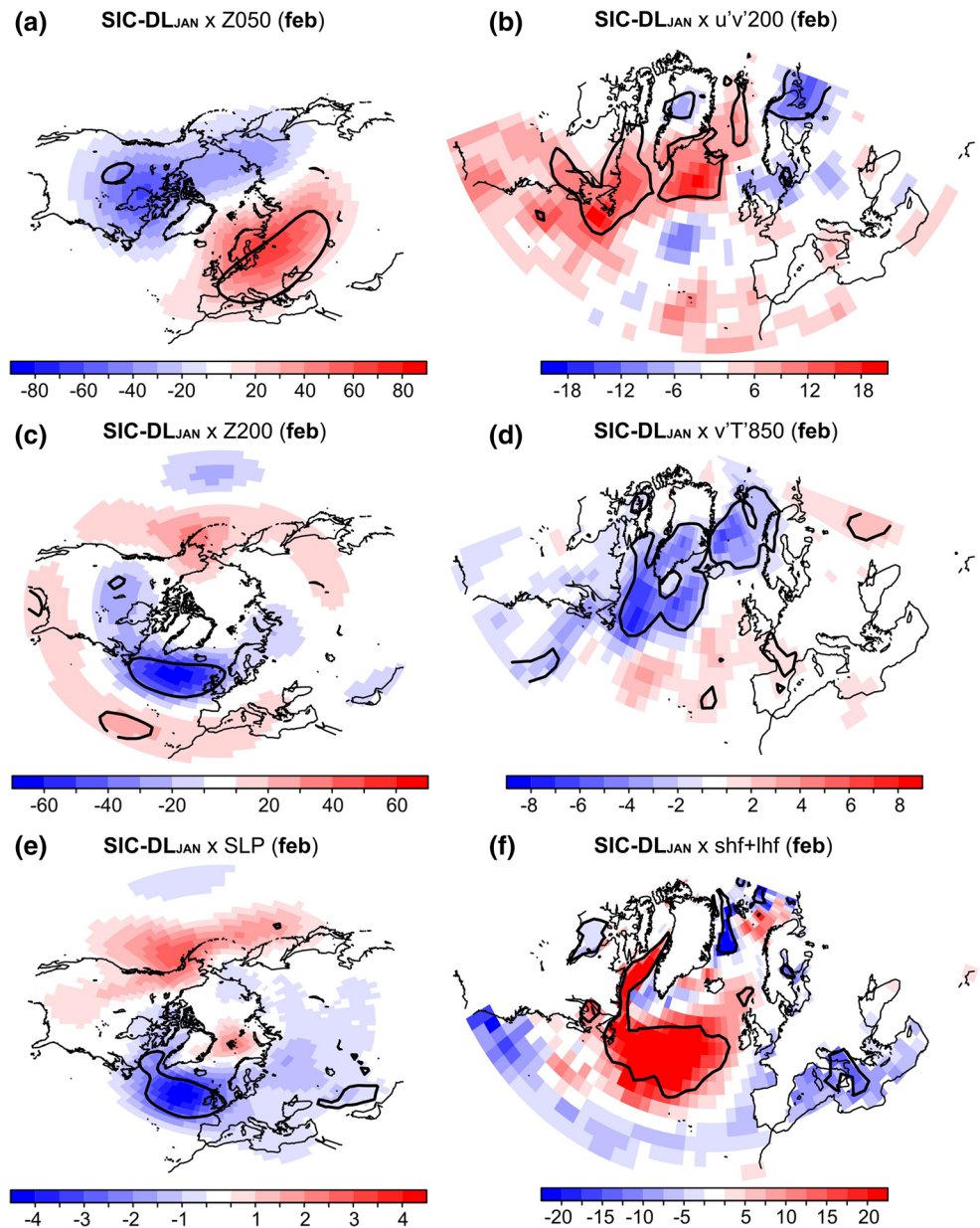
Fig. 7 As Fig. 6, but of transient-eddy momentum flux at 200 hPa (m^2/s^2; *top*), transient-eddy heat flux at 850 hPa (mK/s; *middle*), and surface turbulent heat flux (sensible plus latent, W/m^2; upward is positive; *bottom*)

consistent with the atmospheric response to SIC reduction over the Labrador Sea found by Kvamsto et al. (2004), with negative (positive) geopotential height anomalies at high (middle) latitudes, although their pattern resembled more a NAO-like structure. The regional scale of the anomalous circulation following SIC-DL$_{JAN}$ (Fig. 8c, e) is in qualitative agreement with the regional response to sea-ice changes west of Greenland reported by Magnusdottir et al. (2004), particularly as compared to the hemispheric response to

sea-ice variations east of Greenland (their Fig. 3; see also discussion in Deser et al. 2004), but the sign is opposite in the respective patterns. Composite analysis based on ±1 SD of the SIC-DL$_{JAN}$ index confirms that SIC anomalies are accompanied by an EA-like pattern at tropospheric levels (not shown). At the lower-stratosphere (Fig. 8a), the Z050 regression map of SIC-DL$_{JAN}$ shows a wave-1 structure, however the link to stratospheric dynamics is unclear due to the asymmetry in statistical significance.

Fig. 8 (*left*) As Fig. 6-right; (*right*) as Fig. 9-right, but onto the SIC-DL$_{JAN}$ index

(a) SIC-DL$_{JAN}$ x Z050 (**feb**)

(b) SIC-DL$_{JAN}$ x u'v'200 (**feb**)

(c) SIC-DL$_{JAN}$ x Z200 (**feb**)

(d) SIC-DL$_{JAN}$ x v'T'850 (**feb**)

(e) SIC-DL$_{JAN}$ x SLP (**feb**)

(f) SIC-DL$_{JAN}$ x shf+lhf (**feb**)

4 Conclusions

The relationship between observed monthly winter sea-ice anomalies in the Atlantic basin and lagged Euro-Atlantic atmospheric circulation has been investigated in the 1979–2013 period. The statistical approach followed in this study has led to some interesting results that are summarized below:

- A statistically significant influence of the winter NAO-related SIC anomalies on the atmospheric circulation has been found in two cases for the atmosphere in February, showing that this potential feedback can be detected in observations with monthly data, which is consistent with their long decaying time-scale.

- There appears to be an intra-seasonal behaviour in this potential feedback: with SIC-influence in December dominated by anomalies east of Greenland (maximum amplitude in the Greenland Sea), and SIC-influence in January dominated by anomalies west of Greenland. This feature may be linked to the larger expansion of the climatological sea-ice edge and increase in variability in the Davis Strait-Labrador Sea region, from December to January.

- The atmospheric anomalies lagging sea-ice changes in each sub-basin, at the target month, are likewise different. The NAO-driven SIC anomalies in December are followed in February by a NAO-like pattern of opposite polarity at the surface and a hemispheric signature in the upper-troposphere/lower-stratosphere. But, the NAO-
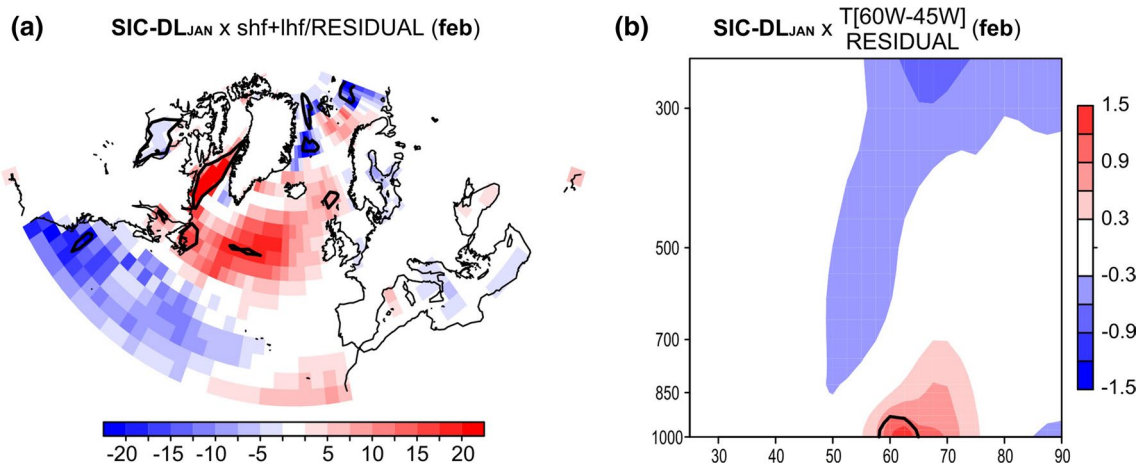
(a) **SIC-DL$_{JAN}$ x shf+lhf/RESIDUAL (feb)**

(b) **SIC-DL$_{JAN}$ x $\dfrac{T[60W\text{-}45W]}{RESIDUAL}$ (feb)**

Fig. 9 Regression of detrended surface turbulent heat flux anomalies (sensible plus latent, W/m^2; upward is positive; **a**) and air–temperature anomalies averaged over 60°W–45°W (pressure level hPa vs latitude °N, K; **b**) in February onto the SIC-DL$_{JAN}$ index after lin-early removing the influence of the EA principal component at each grid-point. Shown are amplitudes associated with one SD of the time-series. Statistically significant areas at 95 % confidence level based on a two-tailed *t* test are *contoured*

driven SIC anomalies in January are then followed by a regional atmospheric anomaly over the North Atlantic that projects on the EA pattern. Transient-eddy activity is likely to be responsible for the settling of these atmospheric anomalies.

A caveat follows. The contribution of the NAO-induced SST anomalies to the Euro-Atlantic atmospheric circulation accompanying sea-ice changes remains to be further examined. Preliminary results, performing multiple-MCA (e.g. Polo et al. 2005) with North Atlantic SST over 80°W–0°E/0°N–70°N as additional predictor field (not shown), suggest that SST anomalies could add to the influence of SIC anomalies east of Greenland in December on the NAO-like atmospheric anomaly in February (sig.lev. for SC 2 %), which is consistent with the discussion on surface heat flux in Sect. 3.2; but deteriorate the covariability between SIC anomalies west of Greenland in January and the EA-like pattern in February (sig.lev. for SC 52 %), which might explain the weaker statistical significance in the corresponding MCA-SIC analysis (Sect. 3.1).

We have described the influence of NAO-related December/January SIC anomalies over the Atlantic basin on the North Atlantic-European circulation in February in terms of *potential* feedback, as the direct boundary forcing is expected to be modest compared to internal atmospheric variability. Hence, sensitivity AGCM experiments prescribing sea-ice removal in each sub-basin would be useful to unambiguously identify the mechanisms at work and the resulting atmospheric response; a coordinated multi-model protocol would be desirable (Cohen et al. 2014; Gao et al. 2015). In addition, coupled GCM experiments with an initial-value approach of the forcing, as in Wu et al. (2007), would allow tracking the joint evolution of SIC/SST anomalies and associated atmospheric response.

In this study, we have taken the convention to analyse atmospheric anomalies following sea-ice reduction in the target Atlantic sub-basin. The results have pointed out that negative SIC anomalies at both side of Greenland, in different months, are associated with distinctive circulation anomalies in the Euro-Atlantic sector. This distinct SIC influence could help interpreting AGCM responses to current or projected sea-ice trends, related to sea-ice decline in both the Greenland-Barents Seas and the Davis Strait-Labrador Sea region, which show conflicting results (e.g. Deser et al. 2010; Screen et al. 2013, 2014).

References

Alexander MA, Bhatt US, Walsh JE, Timlin MS, Miller JS, Scott JD (2004) The atmospheric response to realistic Arctic sea ice anomalies in an AGCM during winter. J Clim 17:890–905

Andrews DG, Holton JR, Leovy CB (1987) Middle atmospheric dynamics. Academic Press, London

Bretherton SB, Smith C, Wallace JM (1992) An intercomparison of methods for finding coupled patterns in climate data. J Clim 5:541–560

Cayan DR (1992) Latent and sensible heat flux anomalies over the Northern Oceans: the connection to monthly atmospheric circulation. J Clim 5:354–369

Chang EKM, Fu Y (2002) Interdecadal variations in Northern Hemisphere winter storm track intensity. J Clim 15:642–658

Cohen J, Screen JA, Furtado JC, Barlow M, Whittleston D, Coumou D, Francis J, Dethloff K, Entekhabi D, Overland J, Jones J (2014) Recent Arctic amplification and extreme mid-latitude weather. Nat Geosci 7:627–637

Comiso JC (2000, updated 2012) Bootstrap sea ice concentrations from Nimbus-7 SMMR and DMSP SSM/I-SSMIS—version 2. Boulder, Colorado USA: NASA DAAC at the National Snow and Ice Data Center

Czaja A, Frankignoul C (2002) Observed impact of Atlantic SST anomalies on the North Atlantic Oscillation. J Clim 15:606–623

Czaja A, Robertson AW, Huck T (2003) The role of Atlantic ocean-atmosphere coupling in affecting the North Atlantic Oscillation variability. In: Hurrell JW, Kushnir Y, Ottersen G, Visbeck M (eds) The North Atlantic Oscillation: climatic significance and environmental impact, vol 134. AGU Geophys Monogr Ser, pp 147–172

Dee DP et al (2011) The ERA-interim reanalysis: configuration and performance of the data assimilation system. Q J R Meteorl Soc 137:553–597

Deser C, Walsh JE, Timlin MS (2000) Arctic sea ice variability in the context of recent atmospheric circulation trends. J Clim 13:617–633

Deser C, Magnusdottir G, Saravanan R, Phillips A (2004) The effects of North Atlantic SST and sea ice anomalies on the winter circulation in CCM3. Part II: direct and indirect components of the response. J Clim 17:877–889

Deser C, Tomas RA, Peng S (2007) The transient atmospheric circulation response to North Atlantic SST and sea ice anomalies. J Clim 20:4751–4767

Deser C, Tomas R, Alexander MA, Lawrence D (2010) The seasonal atmospheric response to projected Arctic sea ice loss in the late twenty-first century. J Clim 23:333–351

Fang Z, Wallace JM (2009) Arctic sea ice variability on a time-scale of weeks and its relation to atmospheric forcing. J Clim 7:1897–1914

Ferreira D, Frankignoul C (2005) The transient atmospheric response to midlatitude SST anomalies. J Clim 18:1049–1067

Frankignoul C (1985) Sea surface temperature anomalies, planetary waves and air–sea feedback in the middle latitudes. Rev Geophys 23:357–390

Frankignoul C, Sennéchael N, Cauchy P (2014) Observed atmospheric response to cold season sea ice variability in the Arctic. J Clim 27:1243–1254

Gan B, Wu L (2015) Feedbacks of sea surface temperature to wintertime storm tracks in the North Atlantic. J Clim 28:306–323

Gao Y, Sun J, Li F, He S, Sandven S, Yan Q, Zhang Z, Lohmann K, Keenlyside N, Furevik T, Suo L (2015) Arctic sea ice and Eurasian climate: a review. Adv Atmos Sci 32:92–114

Hoskins BJ, James IN, White GH (1983) The shape, propagation and mean-flow interaction of large-scale weather systems. J Atmos Sci 40:1595–1612

Hurrell JW, Deser C (2009) North Atlantic climate variability: the role of the North Atlantic Oscillation. J Mar Syst 78:28–41

Hurrell JW, Kushnir Y, Ottersen G, Visbeck M (2003) An overview of the North Atlantic Oscillation. In: Hurrell JW, Kushnir Y, Ottersen G, Visbeck M (eds) The North Atlantic Oscillation: climatic significance and environmental impact, vol 134. AGU Geophys Monogr Ser, pp 1–36

Kvamsto NG, Skeie P, Stephenson DB (2004) Impact of Labrador sea-ice extent on the North Atlantic Oscillation. Int J Climatol 24:603–612

Magnusdottir G, Deser C, Saravanan R (2004) The effects of North Atlantic SST and sea ice anomalies on the winter circulation in CCM3. Part I: main features and storm track characteristics of the response. J Clim 17:857–876

Polo I, Rodríguez-Fonseca B, Sheinbaum J (2005) Northwest Africa upwelling and the Atlantic climate variability. Geophys Res Lett. doi:10.1029/2005GL023883

Screen JA, Simmonds I, Deser C, Tomas R (2013) The atmospheric response to three decades of observed Arctic sea ice loss. J Clim 26:1230–1248

Screen JA, Deser C, Simmonds I, Tomas R (2014) Atmospheric impacts of Arctic sea-ice loss, 1979–2009: separating forced change from atmospheric internal variability. Clim Dyn 43:333–344

Smith TM, Reynolds RW, Peterson TC, Lawrimore L (2008) Improvements to NOAA's historical merged land–ocean surface temperature analysis (1880–2006). J Clim 21:2283–2296

Strong C, Magnusdottir G, Stern H (2009) Observed feedback between winter sea ice and the North Atlantic Oscillation. J Clim 22:6021–6032

Trenberth KE (1986) An assessment of the impact of transient eddies on the zonal flow during a blocking episode using localized Eliassen-Palm flux diagnostics. J Atmos Sci 43:2070–2087

Visbeck M, Chassignet EP, Curry RG, Delworth TL, Dickson RR, Krahmann G (2003) The ocean's response to North Atlantic Oscillation variability. In: Hurrell JW, Kushnir Y, Ottersen G, Visbeck M (eds) The North Atlantic Oscillation: climatic significance and environmental impact, vol 134. AGU Geophys Monogr Ser, pp 113–145

Wallace JM, Lim GH, Blackmon ML (1988) Relationship between cyclone tracks, anticyclone tracks and baroclinic waveguides. J Atmos Sci 45:439–462

Walsh JE, Johnson CM (1979) An analysis of Arctic sea ice fluctuations, 1953–1977. J Phys Oceanogr 9:580–591

Wettstein JJ, Wallace JM (2010) Observed patterns of month-to-month storm-track variability and their relationship to the background flow. J Atmos Sci 67:1420–1437

Woollings T, Hannachi A, Hoskins B (2010) Variability of the North Atlantic eddy-driven jet stream. Q J R Meteorol Soc 136:856–868

Wu Q, Zhang X (2010) Observed forcing-feedback process between Northern Hemisphere atmospheric circulation and Arctic sea ice coverage. J Geophys Res. doi:10.1029/2009JD013574

Wu L, He F, Liu Z, Li C (2007) Atmospheric teleconnections of tropical Atlantic variability: interhemispheric, tropical–extratropical, and cross-basin interactions. J Clim 20:856–870